Sensors and Materials, Vol. 34, No. 2 (2022) 661–668
MYU Tokyo

S & M 2839

Scintillation Properties of Li-doped ZnO Translucent Ceramic

Toshiaki Kunikata,* Takumi Kato, Daiki Shiratori,
Daisuke Nakauchi, Noriaki Kawaguchi, and Takayuki Yanagida

Nara Institute of Science and Technology, 8916-5 Takayama, Ikoma, Nara 630-0192, Japan

(Received October 8, 2021; accepted November 1, 2021)

Keywords: Li-doped ZnO, scintillation, translucent ceramic, annealing effect, lattice defects

We synthesized a 0.1% Li-doped ZnO translucent ceramic using spark plasma sintering (SPS) and annealed it at 700 or 800 °C in air. The photoluminescence (PL) and scintillation properties of all samples were evaluated. The PL quantum yield (*QY*) and scintillation light yield (*LY*) were improved by annealing owing to the reduction in the number of oxygen defects in comparison with the as-prepared sample. Among the translucent ceramic samples, the sample annealed at 700 °C showed the highest *LY* (5800 ph/5.5 MeV-α); the scintillation *LY* was lower in the sample annealed at 800 °C because of the increase in the number of trap sites.

1. Introduction

Inorganic scintillators, which convert high-energy photons[(1)] or particles[(2)] with an energy of keV to MeV into lower-energy photons, have been playing a major role in many fields of radiation detection, including astrophysics,[(3)] medical imaging,[(4)] security,[(5)] resource exploration,[(6)] environmental monitoring,[(7)] and biology.[(8)] Generally, scintillators are combined with photodetectors.[(9)] When radiation interacts with a scintillator, the scintillator converts the energy of the ionizing radiation to low-energy photons. After these photons are converted to electrons by the photodetector, an electrical signal flows into an electrical circuit, and a computer performs a detailed analysis of the signal.

Scintillators for α-ray detection have been used in nuclear facilities, where uranium and plutonium, which emit α-rays, must be monitored because their absorption by workers could seriously affect their health. Materials with an intermediate effective atomic number (Z_{eff} = 10–30) are used as scintillators for α-ray detection because they do not easily detect environmental γ-rays and background neutrons. Thus, Ag-doped ZnS (ZnS:Ag) has been applied in most scintillation detectors for α-rays for many years.[(10)] However, ZnS:Ag is only available as a white polycrystalline powder and must be sprayed on thin opaque screens, resulting in its energy resolution being insufficient to separate various radioisotopes.[(11)] One of the reasons for the low energy resolution of ZnS:Ag is its opacity, and alternative materials with high transmittance are desirable to achieve a higher energy resolution.

*Corresponding author: e-mail: kunikata.toshiaki.kt1@ms.naist.jp
https://doi.org/10.18494/SAM3683

ISSN 0914-4935
https://myukk.org/

ZnO is a promising next-generation α-ray detector since Z_{eff} of ZnO is close to that of ZnS:Ag. ZnO has mostly been studied for its use in semiconductor devices such as LEDs,[12] although other phosphor applications, including scintillators, are expected, similarly to other semiconductor materials such as GaN[13] and Ga_2O_3.[14] In terms of its scintillation properties, ZnO shows two types of luminescence: sub-nanosecond luminescence due to free excitons at around 390 nm[15] and microsecond-order luminescence due to lattice defects in the visible region.[16] Some researchers have explored luminescence due to free excitons and reported a scintillation light yield (*LY*) of In-doped ZnO thin film of 625 ph/5.5 MeV-α.[17–19] However, detectors do not always require such a fast response from free excitons. For example, the scintillation of ZnS:Ag has a decay time constant of microsecond order.[20] On the other hand, other researchers have reported a scintillation *LY* due to the lattice defects of Cd-doped ZnO thin film of 18000 ph/5.5 MeV-α.[21] In most environments in which *α*-ray scintillation detectors are employed, the counting rate of *α*-rays is not high, and microsecond-order decay is acceptable. Thus, ZnO with enhanced lattice-defect luminescence is potentially suitable for this application.

In this study, we focused on a translucent ceramic,[22–24] a new material form of scintillators that can be used to enhance lattice-defect luminescence. Translucent ceramics have more lattice defects than other material forms such as single crystals,[25,26] which are generally used as scintillators; thus, ZnO translucent ceramics may have enhanced *LY*. Moreover, it was previously reported that the introduction of Li increased the concentration of lattice defects and enhanced the photoluminescence (PL) properties of ZnO films.[27] Thus, Li doping into ZnO may also enhance scintillation properties. In addition, it has been reported that annealing regulated the amount of lattice defects in ZnO and enhanced the lattice-defect luminescence.[16,28] Therefore, we prepared 0.1% Li-doped ZnO translucent ceramic by spark plasma sintering (SPS) and annealed samples in air, then evaluated their PL and scintillation properties.

2. Materials and Methods

2.1 Sample preparation

The Li-doped ZnO translucent ceramic was synthesized by SPS (SinterLand LabX-100) in a vacuum.[29] First, raw powders of ZnO (99.99%, Kojundo Chemical) and Li_2CO_3 (99.99%, Rare Metallic) were mixed with a mortar and pestle. The mass of the mixture was 0.5 g and the Li concentration was fixed to 0.1 mol%. Then, the Li-doped ZnO powder was poured into a cylindrical graphite die with a hole of 10.4 mm diameter, which was held between two graphite punches. The sintering sequence was as follows. First, the temperature was increased from 20 to 600 °C in 5 min, then kept at 600 °C for 5 min under a pressure of 13 MPa. Next, the sintering temperature was increased from 600 to 1100 °C in 50 min and kept at 1100 °C for 20 min under a pressure of 100 MPa. After the sintering, the surface of the translucent ceramic was polished using a polishing machine (MetaServ 250, BUEHLER), after which the thickness of the translucent ceramic was approximately 0.5 mm. Then, we divided the translucent ceramic into three pieces, two of which were annealed for 24 h in air, one at 700 °C and the other at 800 °C.

2.2 Evaluation methods

Diffuse transmittance spectra from 300 to 800 nm were evaluated using a spectrophotometer (SolidSpec-3700, Shimadzu). PL quantum yields (*QY*s) were recorded using a Quantaurus-QY spectrometer (C11347, Hamamatsu Photonics). PL excitation and emission spectra from 300 to 700 nm were measured using a spectrofluorometer (FP-8600, JASCO). PL decay curves were measured using a Quantaurus-τ spectrometer (C11367, Hamamatsu).

X-ray-induced scintillation spectra in the range of 300–690 nm were measured using our original setup.[30] An X-ray generator (XRB80P&N200X4550, Spellman) was used as the excitation source. The applied tube voltage and current were 80 kV and 1.2 mA, respectively. During irradiation, the scintillation photons were guided into a spectrometer (Andor DU-420-BU2 CCD with a Shamrock 163 monochromator) through an optical fiber. X-ray-induced scintillation decay curves were evaluated using our original setup.[31] To determine the scintillation *LY*s induced by 5.5 MeV α-rays from ^{241}Am, the pulse-height spectra were measured using our original system with a shaping time of 5 μs.[32] To calculate scintillation *LY*s of the Li-doped ZnO samples, we compared them with that of Ce-doped $Y_3Al_5O_{12}$ (YAG:Ce) as a reference sample (12000 ph/5.5 MeV-α)[33] because YAG:Ce has a similar emission wavelength to that of the lattice-defect luminescence of Li-doped ZnO.

Thermally stimulated luminescence (TSL) glow curves were evaluated using a TSL reader (TL-2000, Nanogray Inc.). The Li-doped ZnO samples were irradiated by X-rays of 10 Gy before measuring the TSL glow curve. The measured temperature range was from 50 to 400 °C.

3. Results and Discussion

Figures 1(a) and 1(b) show the samples under room light and UV light illumination (365 nm), respectively. Hereinafter, the Li-doped ZnO sample annealed at 700 °C (800 °C) is referred to as the 700 °C (800 °C) sample. The annealed samples were transparent to the naked eye, and the color changed from dark brown before annealing to light green after annealing. The annealed samples clearly showed orange luminescence under UV illumination at 365 nm. The color of the undoped sample was slightly lighter than that of the Li-doped samples.

Figure 2 shows the diffuse transmittance spectra of the samples. The annealed samples showed an optical absorption edge at 400 nm, which roughly coincided with the bandgap of ZnO. An absorption band was observed from 400 to 550 nm in the as-prepared sample but

(a) (b)

Fig. 1. (Color online) Li-doped ZnO samples under (a) room light and (b) UV light at 365 nm.

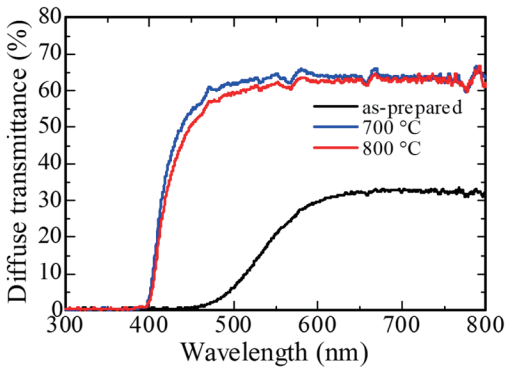

Fig. 2. (Color online) Diffuse transmittance spectra of Li-doped ZnO samples.

not in the annealed samples. This absorption was due to oxygen defects[34] and resulted in the brown color of the as-prepared sample, as shown in Fig. 1(a).

Figure 3 shows the PL excitation and emission spectra. All the samples showed excitation peaks at around 390 nm and broad emission peaks at around 500 nm. Judging from the emission peak positions, the emission peaks were due to lattice defects.[15] For the annealed samples, the excitation and emission peaks were at slightly longer and shorter wavelengths than those of the as-prepared sample, respectively. The *QY*s of the 700 and 800 °C samples were 4.2 and 5.4%, respectively, and the *QY* of the as-prepared sample was below the detection limit (1%) of the instrument. The annealing effect increased the *QY* of the Li-doped ZnO translucent ceramic samples because of the decreased self-absorption. The emission peak at around 500 nm overlapped with the absorption peak at 400–550 nm observed in the diffuse transmittance spectra; thus, the lattice-defect luminescence of the as-prepared sample was strongly affected by the self-absorption. The self-absorption also caused the peak shifts in the PL excitation and emission spectra.

The PL decay curves of the samples are illustrated in Fig. 4. The excitation wavelength was 405 nm, whereas the monitored emission wavelength was 500 nm. The decay curves of the annealed samples were approximated by a sum of three exponential decay functions. The 700 °C sample had decay time constants of 0.432, 1.664, and 9.283 μs, and the 800 °C sample had decay time constants of 0.391, 2.350, and 18.633 μs. On the other hand, the decay curve of the as-prepared sample was not detected owing to the low luminescence intensity. The obtained decay time constants were on the order of microseconds. These values were in approximate agreement with thoes in previous reports.[15] The decay curve was composed of three components corresponding to the different types of lattice defect.[15] However, the specific types of lattice defect corresponding to the three components were unclear because several types of lattice defect have similar emission wavelengths according to previous studies.[16,34]

X-ray-induced scintillation spectra of the samples are illustrated in Fig. 5. All the samples showed scintillation peaks between 500 and 550 nm. The scintillation peak positions of the annealed samples shifted to the shorter-wavelength side with a larger shift than that observed in the PL emission spectra. This was because of the transmission-type measurement geometry

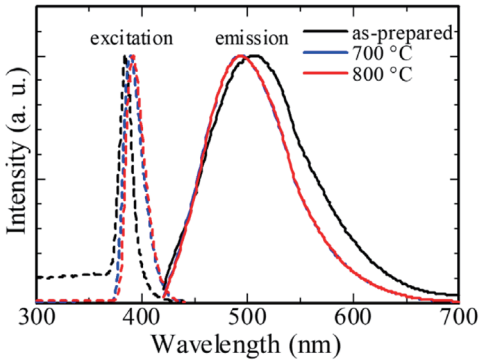

Fig. 3. (Color online) PL excitation and emission spectra of Li-doped ZnO samples.

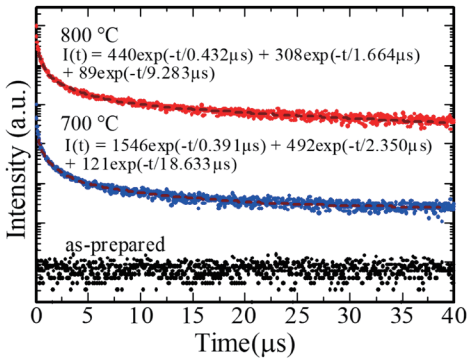

Fig. 4. (Color online) PL decay curves of Li-doped ZnO samples.

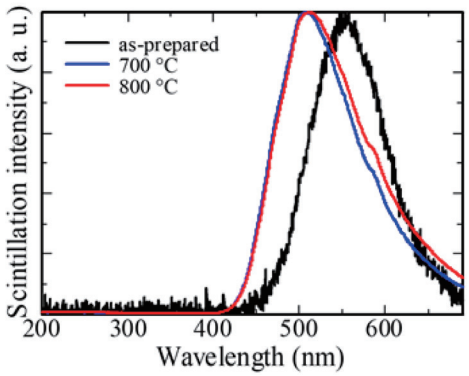

Fig. 5. (Color online) Scintillation spectra of Li-doped ZnO samples under X-ray irradiation.

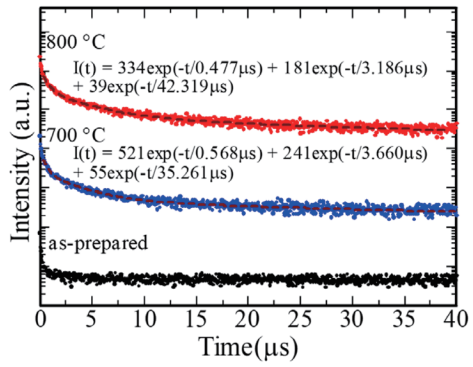

Fig. 6. (Color online) Scintillation decay curves of Li-doped ZnO samples under X-ray irradiation.

used to measure the scintillation spectra, whereas that used to measure the PL spectra was the reflection type. Hence, scintillation is strongly influenced by self-absorption. On the other hand, no exciton luminescence at around 390 nm was observed in all the samples since the excitation wavelength of the lattice-defect luminescence overlaps with the emission wavelength of the exciton luminescence.

X-ray-induced scintillation decay curves of all the samples are shown in Fig. 6. No decay curve was detected for the as-prepared sample because of the low luminescence intensity. The scintillation decay curves of the annealed samples were approximated by a sum of three exponential decay functions in the same manner as for the PL curves. The 700 ℃ sample had decay time constants of 0.477, 3.186, and 42.319 μs, and the 800 ℃ sample had decay time constants of 0.568, 3.660, and 35.261 μs. All the scintillation decay time constants were longer than those for the PL, which can be explained by the different luminescence mechanisms of PL and scintillation. The PL mechanism involves excitation and relaxation processes only at luminescence centers, whereas the scintillation mechanism also includes an energy migration process. Because of this additional process, the scintillation decay time constants are generally longer than those for the PL.

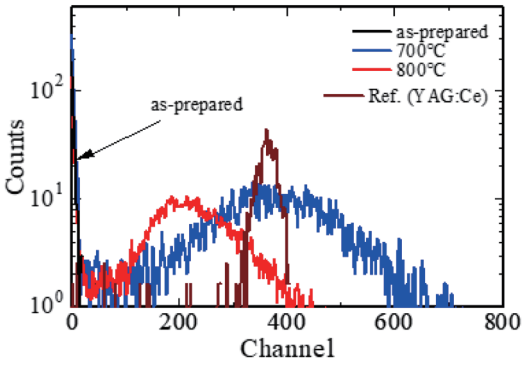

Fig. 7. (Color online) Pulse-height spectra under 241Am α-ray irradiation of Li-doped ZnO samples and YAG:Ce as a reference.

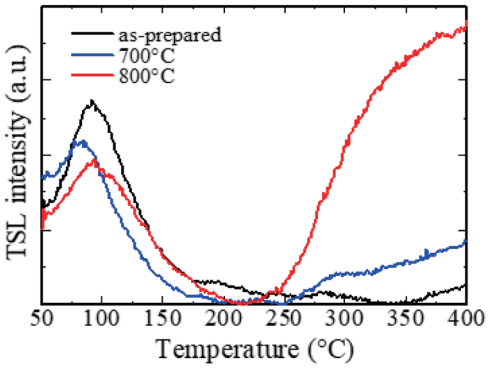

Fig. 8. (Color online) TSL glow curves of Li-doped ZnO samples.

Pulse-height spectra of the samples under α-ray irradiation from ^{241}Am are presented in Fig. 7. Full energy absorption peaks could not be detected for the as-prepared sample. On the other hand, full energy absorption peaks were observed for the annealed samples. The 700 and 800 °C samples showed *LY*s of 5,800 and 3,700 ph/5.5 MeV-α, respectively. These values were higher than that of In-doped ZnO thin film (625 ph/5.5 MeV-α)[17] but lower than that of Cd-doped ZnO thin film (18000 ph/5.5 MeV-α).[21] The 700 °C sample showed a higher *LY* than the 800 °C sample despite the 800 °C sample having the higher *QY*. The phenomenological model of the scintillation mechanism can explain this phenomenon. The *LY* depends on not only the efficiency at luminescence centers (PL *QY*) but also the energy migration efficiency from the host to the luminescence centers and the band gap energy.[35] Therefore, a higher *QY* does not necessarily result in a higher *LY*.

To evaluate the energy migration efficiency indirectly, TSL glow curves were measured. Figure 8 shows TSL glow curves of the samples irradiated with X-rays at 10 Gy. All the samples showed a glow peak at around 100 °C, and the TSL intensity slightly decreased upon annealing. On the other hand, the TSL intensity at 250 °C was much higher for the 800 °C sample than for the 700 °C sample. The 800 °C sample exhibited the largest value of the TSL intensity integrated from 50 to 400 °C. The TSL intensity is related to the number of trap sites; thus, this result suggests that the 800 °C sample has the largest number of trap sites among the three samples. These trap sites deteriorate the energy migration efficiency; thus, the scintillation *LY* of the 800 °C sample was suppressed regardless of its higher PL *QY*. Although we cannot definitively conclude the origin of the trap sites, judging from the transmittance spectra and TSL glow curves, the trap sites at 100 °C may be due to oxygen defects.

4. Conclusions

We synthesized a 0.1% Li-doped ZnO translucent ceramic by SPS. The Li-doped ZnO translucent ceramic showed only lattice-defect luminescence in its PL and scintillation properties. Annealing increased the PL *QY* and scintillation *LY* because it suppressed self-

absorption. The translucent ceramic annealed at 700 °C showed the highest scintillation *LY*; the lower scintillation in the translucent ceramic annealed at 800 °C was due to the increased number of trap sites.

Acknowledgments

This work was supported by Grants-in-Aid for Scientific Research B (19H03533, 21H03733, and 21H03736), Early-Career Scientists (20K15026 and 20K20104), and JSPS Fellows (20J23225) from the Japan Society for the Promotion of Science. The Cooperative Research Project of the Research Center for Biomedical Engineering, Yashima Environment Technology Foundation, Okura Kazuchika Foundation, and Hitachi Metals-Materials Science Foundation are also acknowledged.

References

1 Y. Fujimoto, K. Saeki, D. Nakauchi, T. Yanagida, M. Koshimizu, and K. Asai: Sens. Mater. **31** (2019) 1241.
2 N. Kawaguchi, H. Kimura, M. Akatsuka, G. Okada, N. Kawano, K. Fukuda, and T. Yanagida: Sens. Mater. **30** (2018) 1585.
3 H. Kimura, F. Nakamura, T. Kato, D. Nakauchi, G. Okada, N. Kawaguchi, and T. Yanagida: J. Mater. Sci. Mater. Electron. **29** (2018) 8498.
4 Q. Liu, Y. Cheng, Y. Yang, Y. Peng, H. Li, Y. Xiong, and T. Zhu: Appl. Radiat. Isot. **163** (2020) 109217.
5 I. Kanno, R. Imamura, Y. Yamashita, M. Ohtaka, M. Hashimoto, K. Ara, and H. Onabe: Jpn. J. Appl. Phys. **53** (2014) 056601.
6 C. L. Melcher: Nucl. Inst. Methods Phys. Res., Sect. B **40**–**41** (1989) 1214.
7 K. Watanabe, T. Yanagida, and K. Fukuda: Sens. Mater. **27** (2015) 269.
8 T. Matsubara, T. Yanagida, N. Kawaguchi, T. Nakano, J. Yoshimoto, M. Sezaki, H. Takizawa, S. P. Tsunoda, S. ichiro Horigane, S. Ueda, S. Takemoto-Kimura, H. Kandori, A. Yamanaka, and T. Yamashita: Nat. Commun. **12** (2021) 4097.
9 T. Yanagida: Opt. Mater. (Amst). **35** (2013) 1987.
10 S. A. McElhaney, J. A. Ramsey, M. L. Bauer, and M. M. Chiles: IEEE Trans. Nucl. Sci. **37** (1990) 868.
11 M. Toribio, J. F. García, A. Izquierdo-Ridorsa, R. Tauler, and G. Rauret: Anal. Chim. Acta **310** (1995) 297.
12 K. Nakahara, S. Akasaka, H. Yuji, K. Tamura, T. Fujii, Y. Nishimoto, D. Takamizu, A. Sasaki, T. Tanabe, H. Takasu, H. Amaike, T. Onuma, S. F. Chichibu, A. Tsukazaki, A. Ohtomo, and M. Kawasaki: Appl. Phys. Lett. **97** (2010) 013501.
13 T. Yanagida, T. Kato, D. Nakauchi, G. Okada, and N. Kawaguchi: Appl. Phys. Express **14** (2021) 082006.
14 T. Yanagida, G. Okada, T. Kato, D. Nakauchi, and S. Yanagida: Appl. Phys. Express **9** (2016) 042601.
15 E. I. Gorokhova, S. B. Eron'ko, E. A. Oreshchenko, A. V. Sandulenko, P. A. Rodnyĭ, K. A. Chernenko, I. D. Venevtsev, A. M. Kul'kov, F. Muktepavela, and P. Boutachkov: J. Opt. Technol. **85** (2018) 729.
16 E. I. Gorokhova, G. V. Ananieva, S. B. Eron'ko, E. A. Oreschenko, P. A. Rodnyi, K. A. Chernenko, I. V. Khodyuk, E. P. Lokshin, G. B. Kunshina, O. G. Gromov, and K. P. Loot: J. Opt. Technol. **78** (2011) 753.
17 T. Yanagida, Y. Fujimoto, A. Yoshikawa, Y. Yokota, M. Miyamoto, H. Sekiwa, J. Kobayashi, T. Tokutake, K. Kamada, and S. Maeo: IEEE Trans. Nucl. Sci. **57** (2010) 1325.
18 K. A. Chernenko, E. I. Gorokhova, S. B. Eronko, A. V. Sandulenko, I. D. Venevtsev, H. Wieczorek, and P. A. Rodnyi: IEEE Trans. Nucl. Sci. **65** (2018) 2196.
19 K. A. C. Hernenko, I. D. V Enevtsev, A. M. K. U. L. Kov, F. A. M. Uktepavela, and P. L. B. Outachkov: J. Opt. Technol. **85** (2018) 729.
20 N. Kubota, M. Katagiri, K. Kamijo, and H. Nanto: Nucl. Instrum. Methods Phys. Res., Sect. A **529** (2004) 321.
21 T. Yanagida, Y. Fujimoto, M. Miyamoto, and H. Sekiwa: Jpn. J. Appl. Phys. **53** (2014) 02BC13.
22 T. Kato, D. Nakauchi, N. Kawaguchi, and T. Yanagida: Sens. Mater. **32** (2020) 1411.
23 H. Kimura, T. Kato, D. Nakauchi, N. Kawaguchi, and T. Yanagida: Sens. Mater. **33** (2021) 2187.
24 H. Kimura, T. Kato, D. Nakauchi, N. Kawaguchi, and T. Yanagida: Sens. Mater. **32** (2020) 1381.
25 Y. Takebuchi, H. Fukushima, T. Kato, D. Nakauchi, N. Kawaguchi, and T. Yanagida: Sens. Mater. **32** (2020) 1405.

26 D. Nakauchi, T. Kato, N. Kawaguchi, and T. Yanagida: Sens. Mater. **33** (2021) 2203.
27 M. Hjiri, M. S. Aida, O. M. Lemine, and L. El Mir: Mater. Sci. Semicond. Process. **89** (2019) 149.
28 P. Rodnyi, K. Chernenko, O. Klimova, V. Galkin, A. Makeenko, E. Gorokhova, D. Buettner, W. Keur, and H. Wieczorek: Radiat. Meas. **90** (2016) 136.
29 T. Kato, N. Kawano, G. Okada, N. Kawaguchi, and T. Yanagida: Nucl. Instrum. Methods Phys. Res., Sect. B **435** (2018) 296.
30 T. Yanagida, K. Kamada, Y. Fujimoto, H. Yagi, and T. Yanagitani: Opt. Mater. (Amst). **35** (2013) 2480.
31 T. Yanagida, Y. Fujimoto, T. Ito, K. Uchiyama, and K. Mori: Appl. Phys. Express **7** (2014) 3.
32 T. Yanagida, Y. Fujimoto, M. Arai, M. Koshimizu, T. Kato, D. Nakauchi, and N. Kawaguchi: Sens. Mater. **32** (2020) 1351.
33 H. Takahashi, T. Yanagida, D. Kasama, T. Ito, M. Kokubun, K. Makishima, T. Yanagitanit, H. Yagi, T. Shigeta, and T. Ito: IEEE Nucl. Sci. Symp. Conf. Rec. **3** (2005) 1337.
34 P. A. Rodnyi, K. A. Chernenko, E. I. Gorokhova, S. S. Kozlovskii, V. M. Khanin, and I. V. Khodyuk: IEEE Trans. Nucl. Sci. **59** (2012) 2152.
35 T. Igashira, N. Kawano, G. Okada, N. Kawaguchi, and T. Yanagida: Opt. Mater. (Amst) **79** (2018) 232.